processes

MDPI

Article

Theoretical Study on Critical Liquid-Carrying Capacity of Gas Wells in Fuling Shale Gas Field

Yang Cheng [1,2,3,*], Dajiang Wang [1], Jun Luo [1] and Ruiquan Liao [2,3]

[1] Petroleum Engineering Research Institute, Jianghan Oilfield, Wuhan 430000, China
[2] School of Petroleum Engineering, Yangtze University, Wuhan 430100, China
[3] The Multiphase Flow Laboratory, Gas Lift Innovation Center, CNPC, Wuhan 430100, China
* Correspondence: 18389599309@163.com; Tel.:+86-18062795782

Abstract: The most common type of well in the Fuling shale gas field is the long horizontal section well. Once the energy attenuates, it is difficult to discharge the accumulated liquid. So, it is particularly important to determine the time of accumulation. Through indoor experiments, it was observed that droplets in the gas core flowing under critical conditions and the liquid film adhering to the tube wall cannot be ignored. It was also discovered that the liquid phase on the tube wall can form fluctuations due to the shear effect of the gas phase. Based on the observed distribution of gas–liquid phases in experiments, a critical liquid-carrying velocity calculation method considering the coexistence of droplets and liquid films, as well as the frictional resistance coefficient at the gas–liquid interface under wave morphology, was established. Integrating production data from 106 wells at home and abroad, as well as testing data from the Fuling example well, the new model was validated. The results showed that the new model can accurately diagnose fluid accumulation in different gas fields, with an accuracy rate of 86.8%, and it can provide an accurate diagnosis for fluid accumulation in gas wells in different water-producing gas fields.

Keywords: critical liquid-carrying gas core; entrained liquid film thickness; gas–liquid interface



Academic Editor: Qingbang Meng

Received: 16 October 2024
Revised: 8 February 2025
Accepted: 5 March 2025
Published: 7 March 2025

Citation: Cheng, Y.; Wang, D.; Luo, J.; Liao, R. Theoretical Study on Critical Liquid-Carrying Capacity of Gas Wells in Fuling Shale Gas Field. *Processes* **2025**, *13*, 776. https://doi.org/10.3390/pr13030776

Copyright: © 2025 by the authors. Licensee MDPI, Basel, Switzerland. This article is an open access article distributed under the terms and conditions of the Creative Commons Attribution (CC BY) license (https://creativecommons.org/licenses/by/4.0/).

1. Preface

Affected by the special seepage mechanism of shale gas, the production of gas wells in the Fuling gas field shows the characteristics of a rapid decline in the early stage and low and stable production in the later stage. For most shale gas wells, the phenomenon of wellbore fluid accumulation is particularly common. Due to the low production pressure in the later stage of shale gas fields and the fact that they are all long horizontal wells, a slight accumulation of liquid can lead to difficulties in gas well drainage and a sudden drop in production. In order to take timely drainage and gas production measures and prevent the deterioration of liquid accumulation problems from affecting gas well production, it is necessary to clarify the minimum liquid-carrying velocity of the gas flow, that is, to determine the current production status through the critical liquid-carrying velocity [1,2].

At present, the commonly used critical liquid transport calculation models are mainly divided into the droplet model and liquid film model. The droplet model was proposed by Turner et al. [3–5] in 1969. It assumes that the liquid phase is transported to the surface in the form of spherical droplets. As long as the gas flow can transport the droplets with the largest diameter to the surface, there is no liquid accumulation at the well bottom. After, Turner, Wang Yizhong, Li Min, and others [6,7] believed that there was a deformation of droplets during the process of liquid-carrying by gas flow. They specifically studied

ellipsoidal and spherical cap droplets as their research subjects and conducted a more in-depth investigation into the forces acting on the droplets. Unlike the liquid drop model's approach to determining liquid accumulation, the liquid film [8,9] theory posits that the process of liquid accumulation in gas wells can be viewed as an upward flow of gas and a downward flow of liquid film. Currently, Barnea's liquid film model [10] is widely used, but this method does not consider the uneven distribution of liquid film thickness in deviated gas wells. Currently, most liquid film models [11] assume uniformity in liquid film thickness, overlooking the impact of well inclination on the critical liquid-carrying velocity.

In the diagnosis process of fluid accumulation at the Fuling gas field, it was found that the critical liquid-carrying gas flow rate varies significantly among different gas wells in each block, ranging from 28% to 120% of the calculated value using the Turner model. In practical applications, it has been observed that the accuracy of fluid accumulation judgment varies greatly depending on the model, with a strong geographical influence [12–14]. The primary factors affecting the model's applicability are, on one hand, its failure to consider the situation where droplets cannot persist for an extended period at a certain inclination angle [15–17] and, on the other hand, its oversight of the impact of the fluid production rate in the wellbore on the gas flow's ability to carry liquid [18,19]. For the Fuling shale gas field, the rapid decline in gas production and water yield from the gas wells, as well as the prolonged low-production and low-pressure phase, inevitably affects the accuracy of fluid accumulation judgment under different production conditions due to changes in water yield. At present, the critical liquid-carrying model only considers droplet inversion or liquid film inversion but does not take into account the influence of liquid production rate and well deviation angle. It has been found that the liquid film and droplet exhibit simultaneity, and considering only the inversion of the liquid film or droplet is not comprehensive. Therefore, this paper takes into account the two liquid phase survival modes of droplets and liquid films due to gas flow shear in the critical state and considers the impact of changes in the gas–liquid interface shape on the wetted perimeter, establishing a new critical liquid-carrying velocity model.

2. Gas–Liquid Two Phase Distribution State

The critical liquid-carrying simulation experiment of gas–liquid two-phase flow was carried out in the Key Laboratory of multiphase pipe flow of Yangtze University, and the critical state was observed under the conditions of different pipe diameters and gas–liquid flow rates. Through visual experiments, the dynamic process of liquid-carrying in gas wells is simulated. The experimental device is shown in the Figure 1.

The test uses water and air as the medium, which can effectively simulate the two-phase flow of produced water and natural gas in the wellbore [19,20]. Under normal temperature and pressure, the air is $\rho_g = 1.184\ \mathrm{kg/m^3}$, the aerodynamic viscosity is $\mu_g = 1.184 \times 10^{-5}$ Pa·s, the water density is $\rho_w = 997.05\ \mathrm{kg/m^3}$, and the hydrodynamic viscosity is $\mu_w = 8.9008 \times 10^{-4}$ Pa·s.

Plexiglass tubes with inner diameters of 75 mm and 60 mm were selected for the experiment. The inversion of the liquid film was observed using a high-speed camera, serving as a criterion for determining the critical state of liquid entrainment in the gas flow. The gas flow velocity under different liquid volume conditions was recorded. The experimental process is as follows: ① the liquid phase enters the liquid pipeline from the buffer tank through the plunger pump and liquid flow meter; ② the air enters the gas pipeline after passing through the compressor, buffer tank, and gas flow meter; ③ the two-phase fluid is formed by mixing in the mixer at the front end of the test pipeline and then enters the test section; ④ under a fixed liquid flow rate, adjust the gas volume from high to low, observe the transparent test section until the liquid film at the tube wall falls

back, and record the gas flow velocity at this time as the critical liquid-carrying velocity at that liquid volume; ⑤ adjust the liquid volume, pipeline inclination angle, and diameter multiple times, and repeat the above steps.

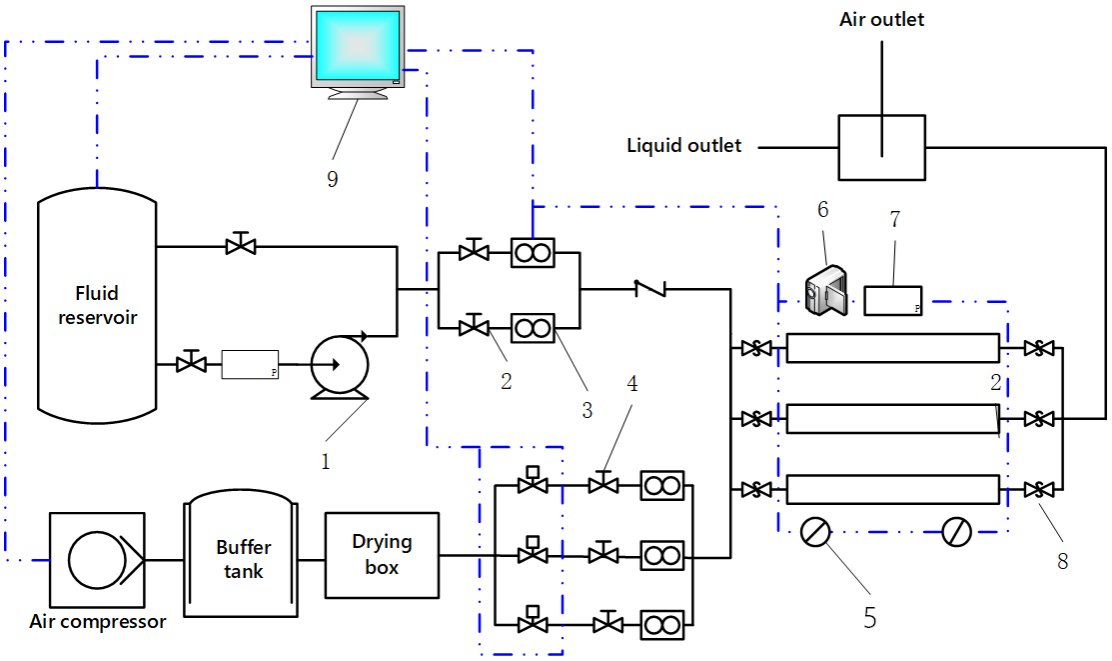

Figure 1. Laboratory device diagram.

The distribution diagram of the gas–liquid two-phase critical state is shown in Figure 2, and it is observed that liquid droplets and liquid films coexist in the critical state.

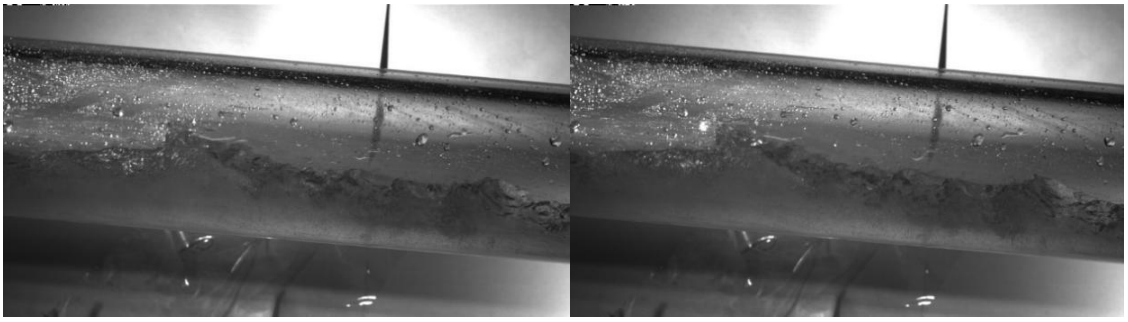

Figure 2. Distribution of gas–liquid phases during critical liquid-carrying under different liquid flow rates.

Under the condition of tangential velocity, surface waves are easily generated at the gas–liquid interface. The limit value of wave generation U_c [21–24] is

$$U_c = \sqrt{\frac{(\rho_1 + \rho_2)(\rho_2 - \rho_1)}{\rho_1 \rho_2} \cdot \frac{g}{k}} \quad (1)$$

ρ_2—the density of the lower fluid in two-phase flow, kg/m^3;
ρ_1—the density of the upper fluid in two-phase flow, kg/m^3;
g—gravitational acceleration, m/s^2.

Due to the stabilizing effect of surface tension, the velocity of surface waves when surface tension is taken into account is [25–27]

$$U_c = \sqrt{\frac{1}{k\rho_1}(k^2\sigma_l + g\rho_2)} \tag{2}$$

$$k = \frac{\sqrt{4\sigma_l g(\rho_1 - \rho_2)(\rho_1 + \rho_2)^2 + \rho_1^2\rho_2^2(u_1 - u_2)^4} + \rho_1\rho_2(u_1 - u_2)^2}{2\sigma_l(\rho_1 + \rho_2)} \tag{3}$$

σ_l—surface tension at gas–liquid interface, dynes/cm;
u_1—velocity of the upper layer fluid in two-phase flow, m/s;
u_2—velocity of the lower layer fluid in two-phase flow, m/s.

The critical liquid-carrying velocity recorded in the experiment is compared with the theoretical value of surface wave generation. As shown in the Figure 3, the yellow line represents the critical liquid-carrying velocity, and the red column represents the limit velocity U_c of surface wave generation. It can be found that the critical liquid-carrying velocity is always higher than the limit velocity U_c of the surface wave generated by the gas–liquid interface disturbance, which indicates that there is a rolling wave at the gas–liquid interface in the critical state [28].

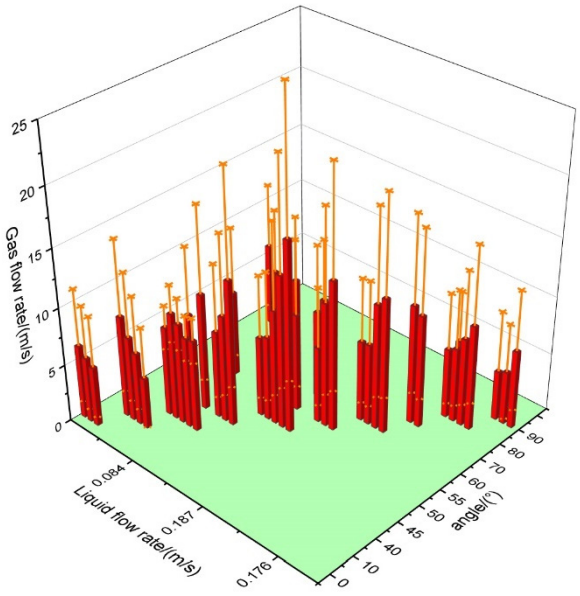

Figure 3. Comparison of critical liquid-carrying velocity and rolling wave threshold.

Through the research of Guner [29] and Adazev [30], it is further confirmed that in the critical liquid-carrying state, the relative velocity between the gas–liquid interface leads to a wavy flow in the liquid phase. The interface morphology of this fluctuation will affect the ability of the airflow to carry liquid and the calculation of the wetted perimeter.

3. Establishment of Theoretical Models

Merely using the liquid film or droplet falling back as the criterion for liquid accumulation cannot accurately describe the gas–liquid two-phase flow under critical liquid-carrying conditions. In the experiment, it was observed that the liquid phase exists simultaneously in the form of droplets and liquid films. The liquid film moves along the pipe wall, while the droplets are carried and transported by the gas phase in mist form. This article aims to establish a critical liquid-carrying model that is more in line with the actual flow state by

considering the situation of liquid droplets carried in the gas core and the liquid film on the pipe wall.

Within an inclined pipeline, due to the circumferential non-uniformity of the liquid film within the inclined pipe, the liquid film primarily accumulates at the bottom of the pipe due to gravity, as shown in Figure 4.

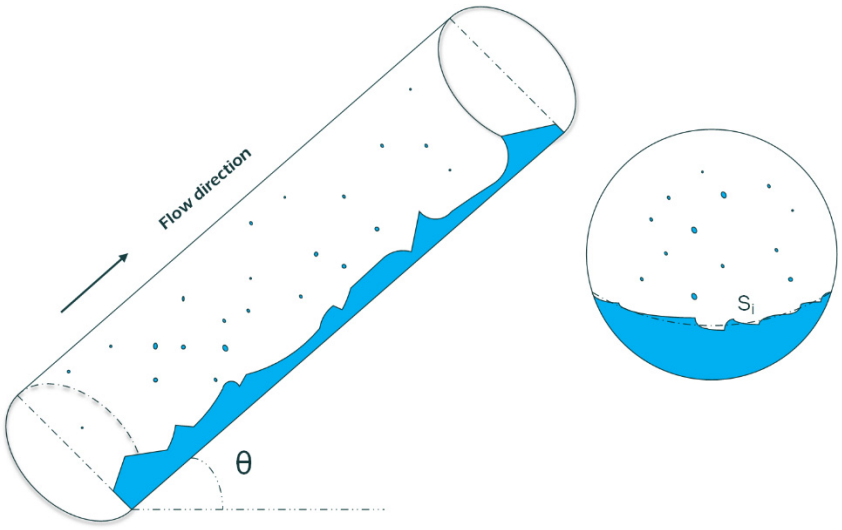

Figure 4. Physical model of critical liquid-carrying state of inclined tube.

Assuming that the sedimentation rate of droplets is equal to the atomization rate of the liquid film under the critical liquid-carrying state, force balance equations are established for both the gas–liquid two-phase flow and the gas phase in the center of the tube, considering the entrainment of droplets in the gas core.

$$-\frac{dp}{dz}A + \tau_w \pi D = \left[\rho_l H_l + \rho_g (1 - H_l)\right] g A sin\theta \tag{4}$$

$$-\frac{dp}{dz}A\left(1 - H_{lf}\right) - \tau_i S_i = \rho_g g A (1 - H_l) sin\theta + \rho_l g A_c H_{lc} sin\theta \tag{5}$$

A—pipe cross-sectional area, m^2;
τ_w—shear force between liquid phase and wall surface, N/m^2;
D—pipe diameter, m;
H_l—liquid holdup;
θ—the angle between the pipeline and the horizontal plane, °;
S_i—wetted perimeter at gas–liquid interface, m;
H_{lf}—the proportion of the liquid phase in the total liquid phase within the liquid film;
τ_i—interphase shear force between gas and liquid phases, N/m^2;
A_c—gas core cross-sectional area, m^2;
ρ_l—liquid phase density, kg/m^3;
ρ_g—gas phase density, kg/m^3.

Under the condition of gas core entraining droplets, the expression for force balance is obtained as follows:

$$\left\{\left[\rho_l H_{lf} + \rho_g (1 - H_l)\right] g A sin\theta - \tau_w \pi D\right\}\left(1 - H_{lf}\right) = \rho_g g A (1 - H_l) sin\theta + \tau_i S_i \tag{6}$$

In Formula (6), the following is calculated:

f_i—friction coefficient;

$$\tau_i = f_i \frac{\rho_g (v_g - v_l)^2}{2} \tag{7}$$

$$H_l = H_{lf} + H_{lc} \tag{8}$$

H_{lc}—ratio of liquid phase in the gas core to total liquid phase.

Since the liquid phase flow rate can be neglected compared to the gas phase flow rate in the critical state, τ_i can be approximated as

$$\tau_i = f_i \frac{\rho_g {v_g}^2}{2} \tag{9}$$

In the critical state, the wall shear stress can be considered as zero, which leads to the calculation model for the critical liquid-carrying flow rate.

$$v_c = \sqrt{\frac{2\left\{\left[\rho_l H_{lf} + \rho_g (1 - H_l)\right]\left(1 - H_{lf}\right) g A sin\theta - \rho_g g A sin\theta (1 - H_l)\right\}}{f_i \rho_g S_i}} \tag{10}$$

Based on the established critical liquid entrainment flow rate calculation model, this article optimizes the calculation methods for three core parameters, namely liquid film holdup, the gas–liquid interface friction coefficient, and the wetted perimeter, according to the described phase distribution of the critical liquid entrainment state.

3.1. Calculation Method for Liquid Film Liquid Holdup

Liquid holdup [31,32] refers to the proportion of the liquid phase area on the flow cross-section to the total flow cross-section. For gas–liquid two-phase flow under critical conditions considering the entrainment of liquid droplets in the gas core, the liquid holdup is derived from the sum of liquid droplets in the gas core and the liquid film on the tube wall.

$$H_l = H_{lc} + H_{lf} \tag{11}$$

In the critical state, assuming that the droplet sedimentation rate is equal to the liquid film atomization rate [14,33] and the droplet entrainment rate reaches dynamic equilibrium, then

$$\frac{F_E / F_{E,max}}{1 - (F_E / F_{E,max})} = \frac{k_A v_{sg} S}{4 k_D} \left[\frac{v_{sg} D^{0.5} (\rho_g \rho_l)^{0.25}}{\sigma_l^{0.5}} - 40 \right]^2 \tag{12}$$

$F_{E,max}$—the limit droplet entrainment rate;
F_E—liquid content in gas core;
v_{sg}—apparent gas velocity, m/s;
v_{sl}—apparent liquid velocity, m/s.

According to the research results of Fore and Dukler et al. [34], the velocity of droplets entrained by the gas core is 80% of the average gas phase velocity; thus, it is believed that S = 0.8 under critical conditions. According to the research of Pan and Hanratty et al. [35], $\frac{k_A v_{sg} S}{4 k_D}$ is approximately equal to the constant 4.8×10^{-5}. The limiting droplet entrainment rate $F_{E,max}$ is calculated using the Al-Sarkhi relationship [36], which is applicable to the low liquid Reynolds number range ($Re_L > 450$) and is closer to the conditions of gas wells with high gas-to-liquid ratios.

$$Re_L = \frac{\rho_L v_{sl} D}{\mu_l} \tag{13}$$

Re_L—the Reynolds number of the liquid phase;
μ_l—gas-phase viscosity, Pa·s.

By combining the above equations, we can obtain the following formula for calculating the droplet entrainment rate:

$$F_E = \frac{\left[1 - e^{-\left(\frac{Re_L}{1400}\right)^{0.6}}\right]\left[v_{sg}\left(\rho_g\rho_l\right)^{0.25}D^{0.5} - 40\sigma_L^{0.5}\right]^2}{1.67 \times 10^4\sigma_L + \left[v_{sg}\left(\rho_g\rho_L\right)^{0.25}D^{0.5} - 40\sigma_L^{0.5}\right]^2} \quad (14)$$

The formula for calculating the liquid holdup of a liquid film is

$$H_{lf} = H_l - H_{lc} = H_l(1 - F_E) \quad (15)$$

H_l adopts the liquid holdup calculation method improved based on the Mukherjee–Brill liquid holdup calculation method [37], using data obtained through long-term measurements of different liquid and gas volumes on the key experimental platform for multiphase pipe flow at PetroChina.For the parameters in the formula, please refer to Table 1.

$$H_l = exp\left[\left(c_1 + c_2 sin\theta + c_3 sin^2\theta + c_4 N_l^2\right)\frac{N_{vg}^{c_5}}{N_{vl}^{c_6}}\right] \quad (16)$$

$$N_{vl} = v_{sl}\left(\frac{\rho_l}{g\sigma}\right)^{0.25} \quad (17)$$

$$N_{vg} = v_{sg}\left(\frac{\rho_l}{g\sigma}\right)^{0.25} \quad (18)$$

$$N_l = \mu_l\left(\frac{g}{\rho_l\sigma^3}\right)^{0.25} \quad (19)$$

Table 1. Liquid holdup coefficient.

Pipe Diameter (mm)	c_1	c_2	c_3	c_4	c_5	c_6
75	−0.2373	−0.1255	0.1042	−0.38899	0.3911	0.02645
60	−0.2351	0.075873	−0.0644	−0.35134	0.447652	0.084494

3.2. Calculation Method of Wetted Perimeter

Due to the consideration of liquid droplets in the gas core and unlike in a vertical tube, the liquid phase flow in an inclined tube is no longer uniformly and symmetrically distributed around the tube wall. More liquid phase accumulates at the bottom of the tube wall, presenting an irregular state, which complicates the calculation method for the wet perimeter of the gas–liquid phase interface.

Wang Wujie [38] et al. believe that the phase interface morphology distribution in the critical state is uncertain. According to the research by E. Roitberg [39,40], capillary forces dominate at low liquid flow rates, making the gas–liquid interface prone to forming a convex shape. At high liquid flow rates, the gas–liquid interface profile begins to exhibit a concave shape, and the rising angle is influenced by the inclination of the pipeline. The surface base thickness is calculated using the dimensionless liquid film base thickness formula for annular mist flow given by Henstock and Hanratty [41], which is applicable to

liquid Reynolds numbers ranging from 20 to 15,100 and oil pipe inner diameters ranging from 12.8 to 63.5 mm.

$$\frac{\delta_L}{D} = \frac{6.59F}{(1+1400F)^{0.5}} \tag{20}$$

$$F = \frac{\gamma}{Re_{sg}^{0.9}} \frac{\mu_l}{\mu_g} \left(\frac{\rho_g}{\rho_l}\right)^{0.5} \tag{21}$$

$$\gamma = \left[\left(0.707 Re_{lf}^{0.5}\right)^{2.5} + \left(0.0379 Re_{lf}^{0.9}\right)^{2.5}\right]^{0.4} \tag{22}$$

$$Re_{sg} = \frac{\rho_g v_{sg} D}{\mu_g} \tag{23}$$

$$Re_{lf} = \frac{\rho_{lf} v_l D}{\mu_l} \tag{24}$$

δ_L—the thickness of the basic liquid film, m;
Re_{sg}—Reynolds number of gas phase;
Re_{lf}—Reynolds number of liquid film;
μ_g—gas-phase viscosity, Pa·s;
ρ_{lf}—liquid film density, kg/m^3.

Based on the experimental data on the base thickness of the liquid film in inclined tubes provided by Paz [42] and Ovadia Shoham [8], a calculation method for the base thickness of liquid film in inclined tubes is established.

From the discussion in the foreword, it can be observed that there are various methods for calculating the critical liquid-carrying flow rate at the current stage. With the increasing application of highly deviated wells and horizontal wells, it is difficult for liquid droplets to persist in inclined wellbores for a long time, making it impossible to use liquid droplet fallback as a criterion for criticality judgment [16]. Through analyzing the critical liquid-carrying test data, it is found that the critical liquid-carrying flow rate is influenced by the angle, and it first increases and then decreases as the angle increases.

As shown in Figure 5, through indoor experiments, this paper conducted densification experiments between 45° and 60° and found that the angle at which airflow is most difficult to carry liquid is 55°. The reason for the occurrence of this angle is that as the angle changes from the vertical segment to the horizontal segment, a thicker liquid film gradually forms at the bottom of the pipe wall, requiring higher gas velocity to prevent the descent of the liquid film. On the other hand, as the pipeline deviates, the gravitational force acting on the liquid phase to fall back decreases, thereby reducing the critical gas velocity. The increase in liquid film thickness and the decrease in gravitational gradient jointly determine the change in critical gas velocity. When the gas wellbore deviates from the vertical position, the influence of the thicker film is greater than the change in the gravitational gradient, thus increasing the critical gas velocity. At approximately 55°, the critical gas flow rate reaches its maximum value. When the deviation angle is greater than 55°, the decrease in the gravitational gradient becomes dominant, causing the critical gas flow rate to decrease with the increase in the deviation angle.

Based on the data and patterns obtained from indoor experiments, with 55° as the most difficult angle for liquid entrainment, the angle correction term of Belfroid is optimized, and the ratio of the liquid film thickness at the bottom of the inclined tube to the average thickness of the liquid film in the vertical tube section under the same flow conditions is established.

$$\frac{h_{F,0^\circ,inc}}{h_{F,aver.,vert}} = \frac{(\sin(1.7\theta))^{0.38}}{0.74} \tag{25}$$

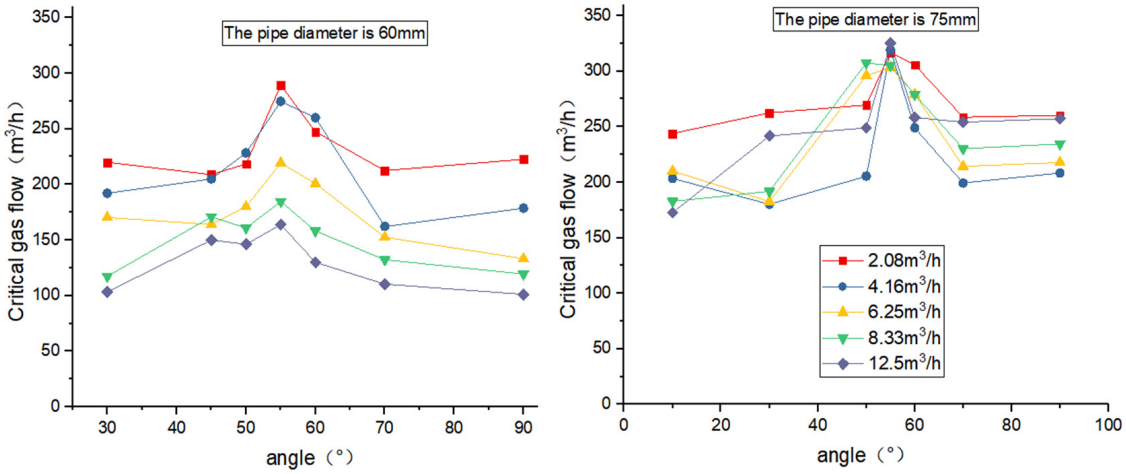

Figure 5. Variation in critical liquid-carrying velocity under different inclination angles of the pipeline.

With the effect of shear force at the gas–liquid interface, the thickness of the newly added liquid film is

$$\Delta\delta = 4000DRe_{sg}^{-1.12} \tag{26}$$

$\Delta\delta$—the thickness of waves, m.

The overall thickness of the liquid film is

$$\delta = \delta_L + \Delta\delta \tag{27}$$

δ—liquid film thickness, m.

Without considering the condition of interfacial waves, the gas–liquid interface contour cannot be determined. According to Wang Wujie [38] et al., the interface can be classified as concave, convex, or planar. However, this paper proves that interfacial fluctuations exist in the critical state; thus, the gas–liquid interface is concave [40]. Therefore, from the perspective of this paper, it is believed that the gas–liquid interface is concave in the critical state, and models where the gas–liquid interface appears convex or planar are considered not to occur under critical conditions.

Hart et al. [41] conducted research on the interface shape of gas–liquid two-phase stratified flow under low-liquid-holdup conditions, obtaining a curved surface model. The key assumption of this model is that the thickness δ_L of the liquid layer remains constant under low-liquid-holdup conditions. The liquid phase wet wall fraction Θ_L is defined, and an empirical relationship for the liquid phase Froude number is proposed.

$$Fr_L = \frac{\rho_L v_{SL}^2}{(\rho_L - \rho_g)gD} \tag{28}$$

$$\Theta = 0.52H_l^{0.374} + 0.26Fr_L^{0.58} \tag{29}$$

Θ—wet wall coefficient;
Fr_l—Froude number of liquid phase.

As shown in Figure 6, with known liquid holdup and liquid film thickness, it is easy to obtain the wet perimeter S_i of the gas–liquid interface.

$$S_i = 2\pi\Theta\left(D/2 - \delta_L / \frac{h_{F,0^\circ,inc}}{h_{F,aver.,vert}}\right) \tag{30}$$

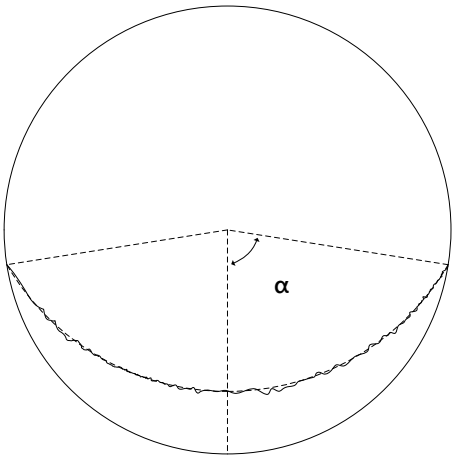

Figure 6. Physical model of gas–liquid interface distribution.

3.3. Friction Coefficient of Gas–Liquid Two-Phase Interface

The friction coefficient at the gas–liquid interface greatly affects the heat, mass, and momentum transfer processes of fluids. Based on the research of domestic and foreign scholars on the friction coefficient of the gas–liquid interface, combined with the classification of key parameters designed by the relationship formula of the gas–liquid interface friction coefficient, it can be roughly confirmed that the factors affecting the friction coefficient of the gas–liquid interface are the Reynolds number, liquid holdup, and liquid film thickness [8]. The "wrinkles" of the interface affect the friction coefficient of the gas–liquid two-phase interface [42]. Therefore, when establishing the calculation method for the friction coefficient of the gas–liquid two-phase interface, on the one hand, the "wrinkles" of the gas–liquid two-phase interface can be equivalent to the roughness of the pipe wall, and on the other hand, the relationship between the critical liquid-carrying velocity and the inclination angle obtained through indoor experiments can be corrected by introducing the inclination angle to adjust the friction factor of the phase interface. This model considers the influence of rolling waves on the gas–liquid interface, but further correction is still needed because conditions do not allow for gas–liquid two-phase flow with multiple tilt angles. f_i [43] must be revised based on indoor gas–liquid two-phase flow experimental data.

$$f_i = 0.005\left\{1 + 300\left[\left(1 + \frac{17500}{Re_{sg}}\right)\frac{\delta_L}{D} - 0.0015\right]\right\} \tag{31}$$

The friction resistance coefficient is generally calculated using the above formula, but this formula does not take into account the influence of rolling waves on the wrinkling of the gas–liquid interface, nor does it consider the influence of the inclination angle on the friction factor of the phase interface. Therefore, introducing the F value facilitates a better calculation of the roughness of the gas–liquid two-phase interface.

$$F = \frac{\delta_L}{D}\left(\frac{u_{sg}}{\sqrt{gD}}\right)\left(\frac{\sigma_l}{\mu_l\sqrt{gD}}\right)^{0.04}\left(\frac{\rho_l g D^2}{\sigma_l}\right)^{0.22}\frac{1.13}{[\sin(1.43\theta)]^{0.4724}} \tag{32}$$

$$f_i = 0.005\left\{1 + 257\left[\left(1 + \frac{17500}{Re_{sg}}\right)\frac{\delta_L}{D}F - 0.0015\right]\right\} \quad (33)$$

4. Application of the New Model in the Fuling Gas Field

Utilizing open-source data provided by Luo [18], Chen Dechun [43], and Ruiqing Ming [44,45] and grounded in a newly established critical fluid carrying model, we conducted a diagnosis of gas well fluid accumulation across various well types, gas–liquid ratios, and gas field production environments. The diagnostic results are illustrated in the Figure 7.

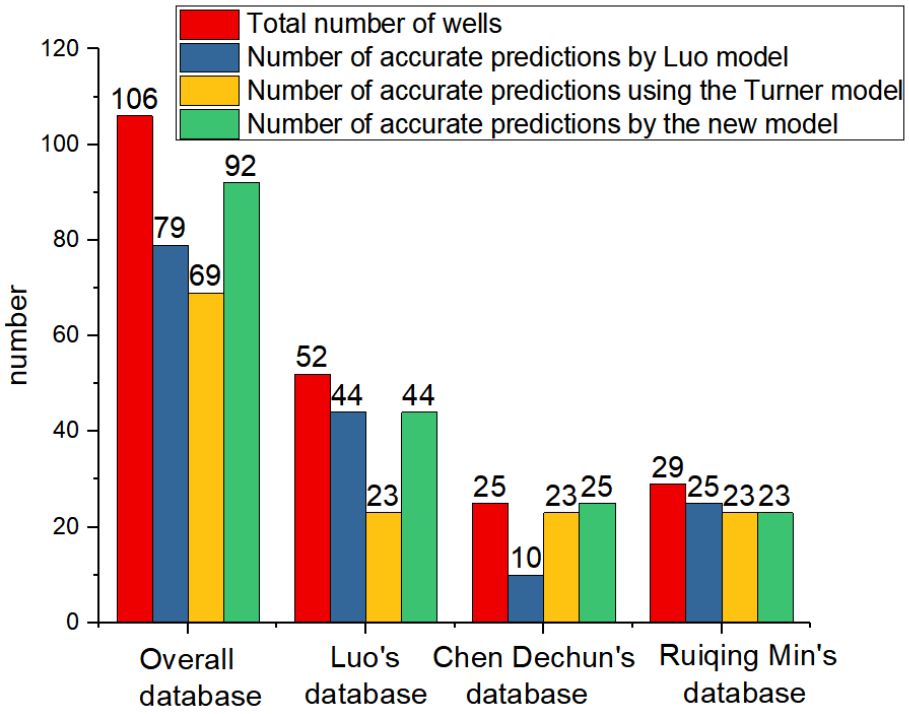

Figure 7. Comparison of model application status.

By collecting production data from 106 well operations across various gas regions worldwide and validating them using the aforementioned models, it was found that different models exhibited varying application scenarios in different gas fields. When applied to the gas field data provided by Luo, the Luo model achieved an accuracy rate of 84.6%. However, when validated against the data provided by Chen Dechun, the accuracy rate dropped to only 40%. Conversely, when applied to the data provided by Ruiqing Ming for fluid accumulation judgment, the accuracy rate reached 86.2%. The average accuracy rate across 106 gas wells was 74.5%. When the Turner model was applied to the gas field data provided by Luo, it achieved an accuracy rate of 46.2%. When applied to the Chen Dechun database, the accuracy rate reached 92%, and when applied to the Ruiqing Ming database, it reached 79.3%. The newly established model achieved an accuracy rate of 84.6% when applied to the gas field data provided by Luo, 100% when applied to the Chen Dechun database, 79.3% when applied to the Ruiqing Ming database, and 86.8% when applied to fluid accumulation judgment for 106 wells. After collecting and comparing the databases, it was found that the newly established model is applicable to different gas fields and production scenarios both domestically and internationally.

The new model has been applied to the diagnosis of fluid accumulation in Well A of the Fuling block. Since Well A was converted from casing flow to tubing production on

14 September 2021, nine flow pressure gradient tests have been conducted. As shown in Figure 8, the results consistently indicate the absence of a fluid level within the wellbore.

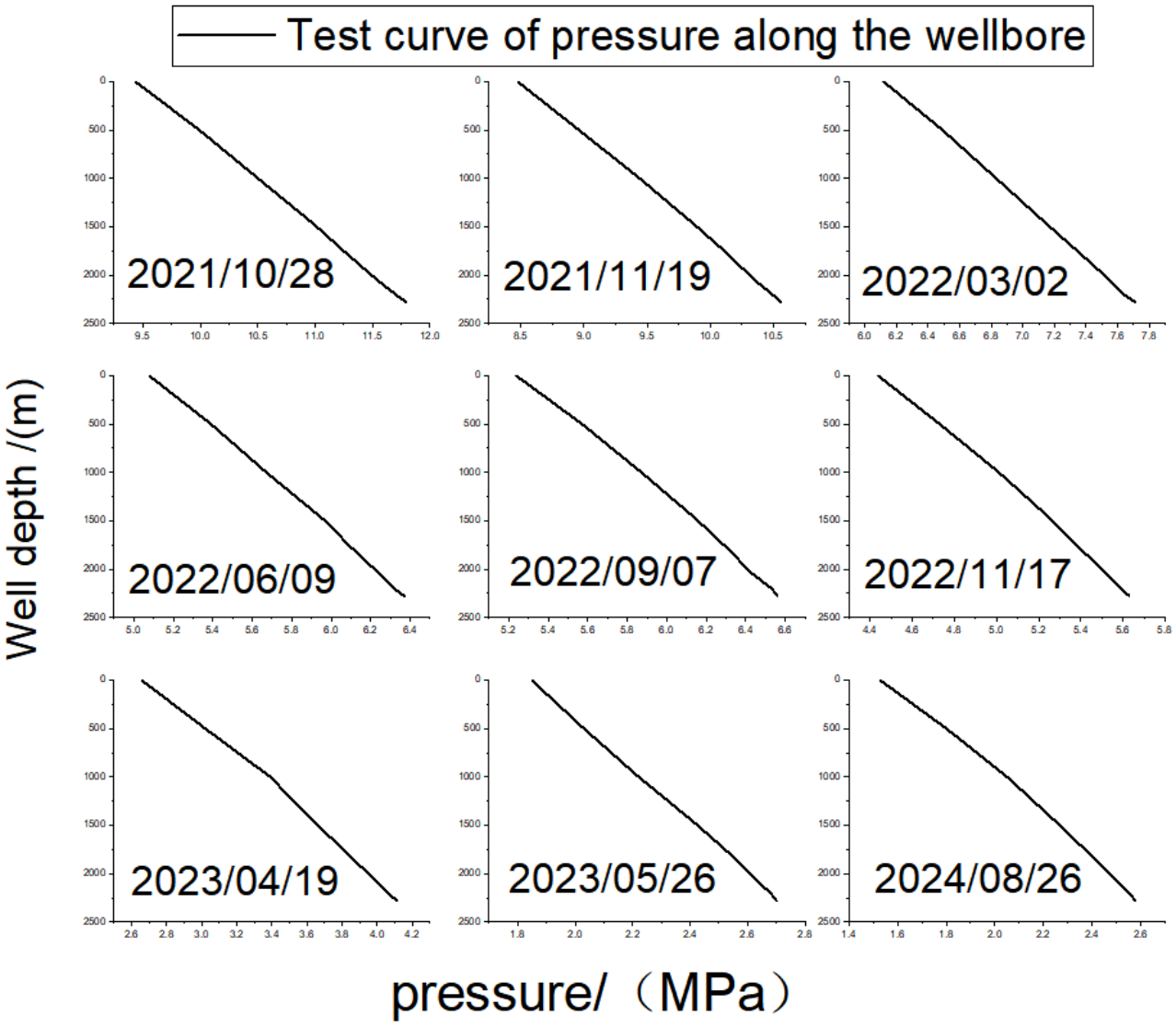

Figure 8. Test results of flow pressure gradient of Well A.

Since the shift to tubing production, frequent operations such as foam displacement, gas lift, and pressure boosting have been adopted. On multiple occasions, it has been determined on-site that the gas well's liquid-carrying capacity is insufficient, indicating that the production status of the gas well is in an unhealthy state.

By utilizing the newly established model to diagnose the fluid accumulation in the actual production conditions of the gas well, it is found that under the current production conditions of Well A, it is not in the healthy production state described by the Turner model, as shown in Figure 9. Considering the current production situation, Well A is currently undergoing enhanced recovery and regularly uses foam gel breakers and gas lift measures. This indicates that fluid accumulation has occurred on-site, but the overall production state remains stable. It can be confidently stated that the newly established model can accurately diagnose the production state of the Fuling gas well.

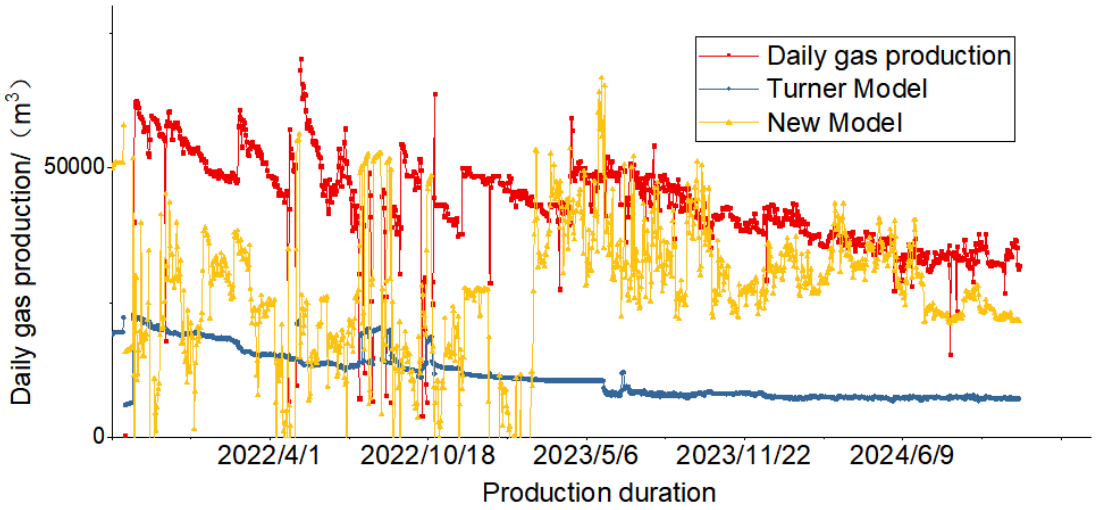

Figure 9. Comparison of fluid accumulation diagnosis throughout the entire life cycle of a gas well.

5. Conclusions

Based on indoor experiments, this paper determines the distribution state under the critical state of the gas–liquid phase and finds that the angle of 55° between the pipeline and the horizontal is the most difficult angle for liquid-carrying. Taking into account the distribution of the liquid phase, the most difficult angle for liquid-carrying, and the fluctuation of the gas–liquid interface, a new model for critical liquid-carrying velocity in gas wells is established. After verification through open-source databases and application in the diagnosis of fluid accumulation in gas wells in the Fuling shale gas field, it is believed that the new model can theoretically describe the critical liquid-carrying velocity in gas wells more accurately. The new model is considered to have good versatility and an accuracy rate of up to 86.8%, meeting the needs of on-site production.

Author Contributions: Conceptualization, Y.C. and R.L.; methodology, Y.C.; software, D.W.; validation, D.W., R.L. and J.L.; formal analysis, Y.C.; investigation, Y.C.; resources, D.W., J.L.; data curation, D.W.; writing—original draft preparation, J.L.; writing—review and editing, J.L., R.L.; visualization, R.L.; supervision, D.W.; project administration, D.W., R.L. All authors have read and agreed to the published version of the manuscript.

Funding: This research received no external funding.

Data Availability Statement: The original contributions presented in the study are included in the article; further inquiries can be directed to the corresponding author.

Conflicts of Interest: Authors: Yang Cheng, Dajiang Wang, and Jun Luo are employed by SINOPEC Petroleum Engineering Research Institute; authors Yang Cheng and Ruiquan Liao are employed by The Multiphase Flow Laboratory of the Gas Lift Innovation Center, CNPC. The authors declare that the research was conducted in the absence of any commercial or financial relationships that could be construed as a potential conflict of interest.

References

1. Zhang, S. Application and assessment of foam drainage and gas production process in Sulige Gas field. *Petrochem. Ind. Technol.* **2017**, *24*, 1.
2. Gao, T.; Wang, G.W.; Shi, S.K. Liquid Loading Diagnosis and Aquifer Size of the Gas Well in Block D of Xushen Gas Field. *Pet. Geol. Oilfield Dev. Daqing* **2017**, *36*, 5.
3. Turner, R.G.; Hubbard, M.G.; Dukler, A.E. Analysis and prediction of minimum flow rate for the continuous removal of liquids from gas wells. *J. Petrol. Technol.* **1969**, *21*, 1475–1482. [CrossRef]
4. Coleman, S.B.; Clay, H.B.; McCurdy, D.G.; Norris, H.L., III. A new look at predicting gas-well load-up. *J. Petrol. Technol.* **1991**, *43*, 329–333. [CrossRef]

5. Coleman, S.B.; Clay, H.B.; McCurdy, D.G.; Norris, H.L., III. Understanding gaswell load-up behavior. *J. Petrol. Technol.* **1991**, *43*, 334–338. [CrossRef]
6. Wang, Y.Z.; Liu, Q.W. A new method to calculate the minimum critical liquids carrying flow rate for gas wells. *Pet. Geol. Oilfield Dev. Daqing* **2007**, *26*, 4.
7. Li, M.; Guo, P.; Tan, G.T. New viewpoint of gas well liquid carrying. *Pet. Explor. Dev.* **2001**, *28*, 105–106.
8. Chen, D.C.; Yao, Y.; Han, H.; Fu, G.; Song, T.J.; Xie, S.X. A new prediction model for critical liquid-carrying flow rate of directional gas wells. *Nat. Gas Ind.* **2016**, *36*, 5.
9. Lei, D.S.; Du, Z.M.; Shan, G.J. Calculation method for critical flow rate of carrying liquid in horizontal gas well. *Acta Pet. Sin.* **2010**, *31*, 637–639.
10. Brauner, N.; Maron, D.M.; Rovinsky, J. A two-fluid model for stratified flows with curved interfaces. *Int. J. Multiph. Flow* **1998**, *24*, 975–1004. [CrossRef]
11. Wang, Q.; Li, Y.C.; Wang, Z.B.; Cheng, J.J. Experimental Study and Model Evaluation on Continuous Liquid Removal in Horizontal Gas Well. *J. Southwest Pet. Univ. (Sci. Technol. Ed.)* **2014**, *36*, 139–145.
12. Wang, Z.B.; Li, Y.C. The Mechanism of continuously removing liquids from gas wells. *Acta Pet. Sin.* **2012**, *33*, 6.
13. Barnea, D. Transition from annualr flow and from dispersed bubble flow-unified models for the whole range of pipe inclinations. *Int. J. Multiph. Flow* **1986**, *12*, 733–744. [CrossRef]
14. Liu, T.; Wang, S.Z.; Guo, X.J.; Pan, G.H.; Chen, H.L.; Wu, Z. New calculation method of gas-liquid two phase annular-mist flow pressure drop of wellbores in gas wells. *Oil Drill. Prod. Technol.* **2017**, *39*, 328–333.
15. Pan, J.; Wang, W.J.; Wang, L.L.; Zhang, L.; Chen, J.B.; Pu, X.L. A prediction model for continuous liquid-carrying in gas wells considering droplet entrainment. *Acta Pet. Sin.* **2019**, *40*, 332–336.
16. Wei, N.; Li, Y.C.; Li, Y.Q.; Liu, A.Q.; Liao, K.G.; Yu, X. Visual experimental Reserch on gas well liquids loading. *Drill. Prod. Technol.* **2007**, *30*, 43–45.
17. Belfroid, S.P.C.; Schiferli, W.; Alberts, G.J.N.; Veeken, C.A.M.; Biezen, E. Prediction onset and dynamic behaviour of liquid loading gas wells. In Proceedings of the SPE Annual Technical Conference and Exhibition, Society of Petroleum Engineers, Denver, CO, USA, 21–24 September 2008.
18. Luo, S.; Kelkar, M.; Pereyra, E.; Sarica, C. A New Comprehensive Model for Predicting Liquid Loading in Gas Wells. *SPE Prod. Oper.* **2014**, *29*, 337–349. [CrossRef]
19. Wang, Q. Experimental Study on Gas-Liquid Flowing in the Wellbore of Horizontal Well. Ph.D. Thesis, Southwest Petroleum University, Chengdu, China, 2014.
20. Van't Westende, J.M.C. Droplets in Annular-Dispersed Gas-Liquid Pipeflows. Ph.D. Thesis, Delft Technical University, Delft, The Netherlands, 2008.
21. Taylor, G.I. The stability of liquid surface when accelerated in a direction perpendicular to their planes I. *Proc. R. Soc. Lond. Ser. A* **1950**, *201*, 192–196.
22. Chandrasekhar, S. *Hydrodynamic and Hydromagnetic Stability*; Clarendon Press: Oxford, UK, 1961; p. 654.
23. Wang, L.F.; Teng, A.P.; Ye, W.H.; Fan, Z.F.; Tao, Y.S.; Lin, C.D.; Li, Y.J. Velocity Gradient Effect of Kelvin Helmholtz Instability of Supersonic Fluid. *Acta Phys. Sin.* **2009**, *58*, 8426–8431.
24. Wang, J. *Two-Dimensional Unsteady Flow and Shock Wave*; China Science Publishing & Media Ltd.: Beijing, China, 1994; pp. 355–356.
25. Wei, P.; Wang, D.; Niu, P.; Pang, C.; Liu, M. A novel centrifugal gas liquid pipe separator for high velocity wet gas separation. *Int. J. Multiph. Flow* **2020**, *124*, 103190. [CrossRef]
26. Hussein, M.M.; Al-Sarkhi, A.; Badr, H.M.; Habib, M.A. CFD modeling of liquid film reversal of two-phase flow in vertical pipes. *J. Pet. Explor. Prod. Technol.* **2019**, *9*, 3039–3070. [CrossRef]
27. Anderitsos, N.; Hanratty, T.J. Interfacial instability for horizontal gas-liquid flow in pipelines. *Int. J. Multiph. Flow* **1987**, *13*, 583–603. [CrossRef]
28. Zhang, Y.J. *Two-Phase Hydrodynamics*; Beihang University Press: Beijing, China, 1987; pp. 469–471.
29. Guner, M.; Pereyra, E.; Sarica, C.; Torres, C. An experimental study of low liquid loading in inclined pipes from 90° to 45°. In Proceedings of the SPE Production and Operations Symposium, Oklahoma City, OK, USA, 1–5 March 2015.
30. Adazev, E. *Two-Phase Annular Flow in Vertical Pipes*; King Fahd University of Petroleum and Minerals: Dhahran, Saudi Arabia, 2018.
31. Pan, J.; Pu, X.L.; Wang, W.J. A prediction model for the critical liquid-carrying velocity of gas-liquid stratified flow in micro-tilting line pipes with low liquid contents. *Nat. Gas Ind. B* **2019**, *39*, 124–133. [CrossRef]
32. Chen, J.L.; Chen, T.P. *Gas Liquid Two-Phase Pipe Flow in Petroleum Industry*; Petroleum Industry Press: Beijing, China, 2010; pp. 4–5.
33. Li, J.C.; Deng, D.M.; Shen, W.W.; Gao, Z.Y.; Gong, J. Mechanism of gas well liquid loading and a new model for predicting critical gas velocity. *Acta Pet. Sin.* **2020**, *41*, 12.
34. Huang, B.; Li, X.H.; Tang, B.Q.; Fu, C. Critical gas velocity model of gas well considering liquid film entrainment mechanism. In Proceedings of the 31st National Natural Gas Academic Annual Conference (2019) (02 Gas Reservoir Development), Hefei, China, 30 October 2019.

35. Pan, L.; Hanratty, T.J. Interpretation of atomization rates of the liquid film in gas liquid annular flow. *Int. J. Multiph. Flow* **2002**, *28*, 363–384. [CrossRef]
36. Al-Sarkhi, A.; Sarica, C.; Qureshi, B. Modeling of droplet entrainment in co-current annular two-phase flow: A new approach. *Int. J. Multiph. Flow* **2012**, *39*, 21–28. [CrossRef]
37. Cheng, Y.; Wu, R.D.; Liao, R.Q.; Liu, Z.L. Study on Calculation Method for Wellbore Pressure in Gas Wells with Large Liquid Production. *Processes* **2022**, *10*, 685. [CrossRef]
38. Roitberg, E.; Shemer, L.; Barnea, D. Application of a borescope to studies of gas–liquid flow in downward inclined pipes. *Int. J. Multiph. Flow* **2006**, *32*, 499–516. [CrossRef]
39. Ullmann, A.; Brauner, N. Closure relations for two-fluid models for two-phase stratified smooth and stratified wavy flows. *Int. J. Multiph. Flow* **2005**, *32*, 82–105. [CrossRef]
40. Wang, W.J.; Cui, G.M.; Wei, Y.Q.; Pan, J. A new model for predicting the critical liquid-carrying velocity in inclined gas wells. *Pet. Explor. Dev.* **2021**, *48*, 1053–1060. [CrossRef]
41. Hart, J.; Hamersma, P.J.; Fortuin, J.M.H. Correlations predicting frictional pressure drop and liquid holdup during horizontal gas liquid pipe flow with a small liquid holdup. *Int. J. Multiph. Flow* **1989**, *15*, 947–964. [CrossRef]
42. Grolman, E.; Fortuin, J. Gas-liquid flow in slightly inclined pipes. *Chem. Eng. Sci.* **1997**, *52*, 4461–4471. [CrossRef]
43. Walls, G.B. *One-Dimensional Two-Phase Flow*; McGraw Hill: New York, NY, USA, 1969.
44. Ming, R.Q.; He, H.Q.; Hu, Q.F. A new predicting method of the critical liquid-loading flow rate for horizontal gas wells. *Pet. Geol. Oilfield Dev. Daqing* **2018**, *37*, 81–85.
45. Fadairo, A.; Olugbenga, F.; Sylvia, N.C. A new model for predicting liquid loading in a gas well. *J. Nat. Gas Sci. Eng.* **2015**, *26*, 1530–1541. [CrossRef]

Disclaimer/Publisher's Note: The statements, opinions and data contained in all publications are solely those of the individual author(s) and contributor(s) and not of MDPI and/or the editor(s). MDPI and/or the editor(s) disclaim responsibility for any injury to people or property resulting from any ideas, methods, instructions or products referred to in the content.